Differential Angular Distribution of H and H^+ Dissociation Fragments of Fast H_2^+ Ions Incident on H_2 Gas*

G. W. McClure
Sandia Laboratory, Albuquerque, New Mexico
(Received 19 April 1965)

Angular distributions of the fast H and H^+ dissociation fragments produced in single collisions of H_2^+ with H_2 have been measured in the energy range 5–80 keV. The observed distributions are discussed in terms of three dissociation reactions, $H_2^+ \rightarrow H^+ + H$, $H_2^+ \rightarrow H^+ + H^+ + e$, and $H_2^+ + e \rightarrow H + H$, whose relative proportions vary strongly over the energy range of the investigation. Distributions of the component of velocity of the dissociation fragments transverse to the H_2^+ beam direction are deduced from the measurements. The H-atom transverse velocity distributions are approximately independent of H_2^+ projectile energy and are dominated by H atoms from the H+H dissociation reaction. The H^+ transverse velocity distributions vary in width as the H_2^+ ion energy is varied. At low energies, where the H^+ production is dominated by the $H^+ + H$ reaction, the transverse velocity spread is narrower than at high energies where the $H^+ + H^+ + e$ reaction dominates the H^+ production. A theory of the dissociation mechanism which predicts the angular distribution of dissociation fragments is developed. The theory is based upon Born-approximation calculations of the dissociation cross section versus internuclear axis orientation and internuclear spacing of the H_2^+ ions prior to the collision. These calculations, presently available only for the case of an H-atom target and for the $1s\sigma_g \rightarrow 2p\sigma_u$ dissociative transition of the incident H_2^+ ion, were used to deduce the angular distribution of dissociation fragments in the laboratory coordinate system. Fairly comprehensive agreement is found between the calculated distribution and the observed H^+ distribution for an H_2 target at 10 keV where the $H + H^+$ dissociation mode dominates the H^+ production. The theoretical model is used to discuss qualitatively the observed shapes and widths of the H^+ and H transverse velocity distributions and to relate qualitatively the shapes of these distributions to the distribution of H_2^+ ion internuclear spacings prior to the collision.

I. INTRODUCTION

When H_2^+ ions in the 10–100 keV kinetic-energy range undergo dissociative collisions, the H and H^+ fragments scatter, on the average, through angles of the order of a degree.[1–4] It has been pointed out[1,3] that the breadth of the scattering is roughly of the size to be expected from electronic excitation of the molecule ion to a state possessing a repulsive internuclear potential. The phenomenon of transverse spreading of the dissociation fragments appears to be closely related to the phenomenon of Aston banding, observed in mass spectrometers, which discloses a spread in the dissociation-fragment velocity components parallel to the initial direction of ion motion.[5–7]

Existing analyses of the electronic-dissociation process[1,3,5–7] invoke the Franck-Condon principle and the assumption that the initial internuclear spacing is approximately that corresponding to the minimum of the $1s\sigma_g$ internuclear-potential curve of H_2^+. If one attempts to refine thsee very rudimentary ideas, it becomes clear that the detailed shape of the angular distribution must depend upon the following: (1) the statistical distribution of internuclear spacings in the incident H_2^+ ions, particularly as affected by the initial vibrational state, (2) the excess energy of the final electronic state as a function of internuclear spacing, and (3) the cross section for excitation to the final repulsive state as a function of internuclear spacing and molecule-axis orientation. To arrive at a through understanding of the dissociation process, a more refined theoretical analysis based on these considerations is needed. Also, a more precise set of measurements of the dissociation-fragment angular distributions is needed to provide a check on the theory. The H_2^+ ion is a natural choice of projectile particle for such work because of its structural simplicity.

The only quantitative information published on the angular distribution of H_2^+ dissociation fragments is that of Damodaran[1] for H_2^+ incident on H_2, N_2, and argon; Fedorenko *et al.*,[2] for H_2^+ incident on argon; Sweetman[3] for H_2^+ incident on H_2, and Barnett[4] *et al.*, for H_2^+ incident on H_2O. These investigations leave many questions unanswered concerning the detailed shape of the differential angular distributions, the differences between the H^+ ion and H atom distributions, and the energy dependence of these distributions. It is one purpose of the present work to provide additional information on these aspects of the dissociation process with H_2 as the target gas.

Measurements were performed in the kinetic-energy range 5 to 80 keV wherein several modes of dissociation are possible. It is convenient to define these modes in

* This work was supported by the U. S. Atomic Energy Commission.

[1] K. K. Damodaran, Proc. Roy. Soc. (London) **239**, 382 (1957).

[2] N. V. Fedorenko, V. V. Afrosimov, R. N. Il'in, and D. M. Kaminker, Zh. Eksperim. i Teor. Fiz. **36**, 385 (1959) [English transl.: Soviet Phys.—JETP **9**, 267 (1959)].

[3] D. R. Sweetman, Proc. Roy. Soc. (London) **A256**, 416 (1960).

[4] C. F. Barnett, M. Rankin, and J. A. Ray, *Proceedings of the Sixth International Conference on Ionization Phenomena in Gases* (Paris, 1963), Vol. I, p. 63.

[5] W. McGowan and L. Kerwin, Can. J. Phys. **41**, 316 (1963).

[6] R. Caudano, J. M. Delfosse, and J. Steyeart, Ann. Soc. Sci. Bruxelles **76**, 127 (1963).

[7] K. H. Purser, P. H. Rose, N. B. Brooks, R. P. Bastide, and A. B. Whittkower, Phys. Letters **6**, 176 (1963).

the notation used by Sweetman[3] and Guidini[8]:

$$H_2^+ \rightarrow H+H^+, \quad \text{reaction 1},$$
$$H_2^+ \rightarrow H^++H^++e, \quad \text{reaction 2},$$
$$H_2^++e \rightarrow H+H, \quad \text{reaction 3}.$$

The process

$$H_2^++e \rightarrow H_2, \quad \text{reaction 4},$$

results in the production of fast H_2 molecules which must be distinguished from the H-atom dissociation products of reactions 1 and 3. The reaction cross sections corresponding to reactions 1 to 4, denoted σ_1, σ_2, σ_3, and σ_4, respectively, have been measured by Sweetman[3] at energies above 100 keV, while Guidini has measured σ_1, σ_2, and $\sigma_3+\sigma_4$ at energies above 30 keV. In interpreting our results, we rely on the Guidini measurements for establishing the relative magnitudes of the various modes.

Theoretical calculations of the cross section for H_2 dissociation in several monatomic gases have been made by Salpeter.[9] This work was relatively rough in that the calculation was semiclassical and the initial and final states of the H_2^+ bound electron were treated in an inexact way. Also, a fixed nuclear spacing of the H_2^+ ion prior to the collision was assumed. It is now quite clear[10] that the initial vibrational state has an effect on the dissociation process. Both vibrational and electronic excitation were considered in the Salpeter treatment and the latter was shown to dominate at high energies. The Salpeter method of treating vibrational dissociation is used in connection with the discussion of the present results to show that this process is relatively unimportant even in the present energy range.

The Born approximation calculations of Peek,[10] giving cross sections for the excitation of H_2^+ ions to the $2p\sigma_u$ dissociative state by electron impact, have been extended recently[11] to the case of H_2^+ collisions with H atoms. The cross section was calculated by Peek at the author's request for an H_2^+ ion kinetic energy of 10 keV as a function of the two variables: internuclear separation in the molecule ion, and the orientation of the molecule ion.[12] The author has derived a laboratory angular distribution of dissociation fragments from these calculations and the results are herewith compared with the experimental results for H_2^+ ions incident on H_2 molecules at 10 keV.

The apparatus and results are discussed in Secs. II and III. Modes of dissociation and their energy dependence are discussed in Sec. IV. The transverse velocity distributions of the dissociation fragments are discussed in Sec. V. Section VI presents the theory and Sec. VII is a discussion of the implications of the present results concerning the accuracy of previous total cross-section measurements.

II. APPARATUS

The apparatus used earlier for the determination of H_2^+ total cross sections[13] was employed in the present work because its proportional-counter detector and post-collision electrostatic deflection system provided the features needed to distinguish the H, H^+, and H_2 products of reactions 1–4. The only modification to the earlier apparatus was a reduction of the detector aperture to a smaller rectangle of dimensions 0.001 $\times$0.010 in. to improve the angular resolution. With this change incorporated, the over-all angular resolution varied linearly from 0.18° to 0.31° as the detector angle was varied from 0° to 2.58°. Over this range of detector angles, the entire collision region was in full view from the detector window and no corrections needed to be made for blockage of the secondary particles by the collision-chamber exit aperture.

All angular distributions presented here are differences between distributions taken at two different collision-chamber pressures (2×10^{-4} and 2×10^{-5} mm Hg) and are therefore free from any significant spurious contribution due to scattering by residual gases (partial pressure 5×10^{-7} mm Hg) or by the collision-chamber slits. It was ascertained in previous studies[13] utilizing the same range of collision-chamber pressures that the total intensity of the secondary particle beams varied linearly with collision-chamber pressure. It was therefore assured that no appreciable multiple scattering was involved under the present operating conditions.

III. RESULTS

The experimental results are shown in Fig. 1. Absolute differential cross sections were determined by integrating the relative differential cross sections and fitting the integrals to the total cross sections measured previously.[13] Only slight variations in the normalization factor were required for the 10 angular distributions, indicating consistency of the present energy dependence of the particle yields with the previous data.

The relative accuracy of the experimental points at each energy was largely governed by the standard deviation of the number of recorded particle counts. This was generally less than 3% in the central portions of the angular distributions and about 20% at the outer extreme of the angular range where the count rates were relatively low. The absolute accuracy of the differential cross sections is estimated as $\pm$20%.

[8] J. Guidini, Compt. Rend. **253**, 829 (1961).
[9] E. E. Salpeter, Proc. Roy. Soc. (London) **A63**, 1295 (1950).
[10] J. M. Peek, Phys. Rev. **134**, A877 (1964).
[11] J. M. Peek, Phys. Rev. **140**, A11 (1965).
[12] The cross-section-versus-orientation calculation was performed by J. M. Peek using a method developed by T. A. Green (unpublished). One requires for the present purpose a cross section as a function of projectile ion orientation relative to the precollision projectile momentum vector $\mathbf{k}_0$ rather than with respect to the momentum transfer vector $\mathbf{k}$ referred to in Ref. 10. The calculation was carried out with linear-combination-of-atomic-orbitals wave functions.
[13] G. W. McClure, Phys. Rev. **130**, 1852 (1962).

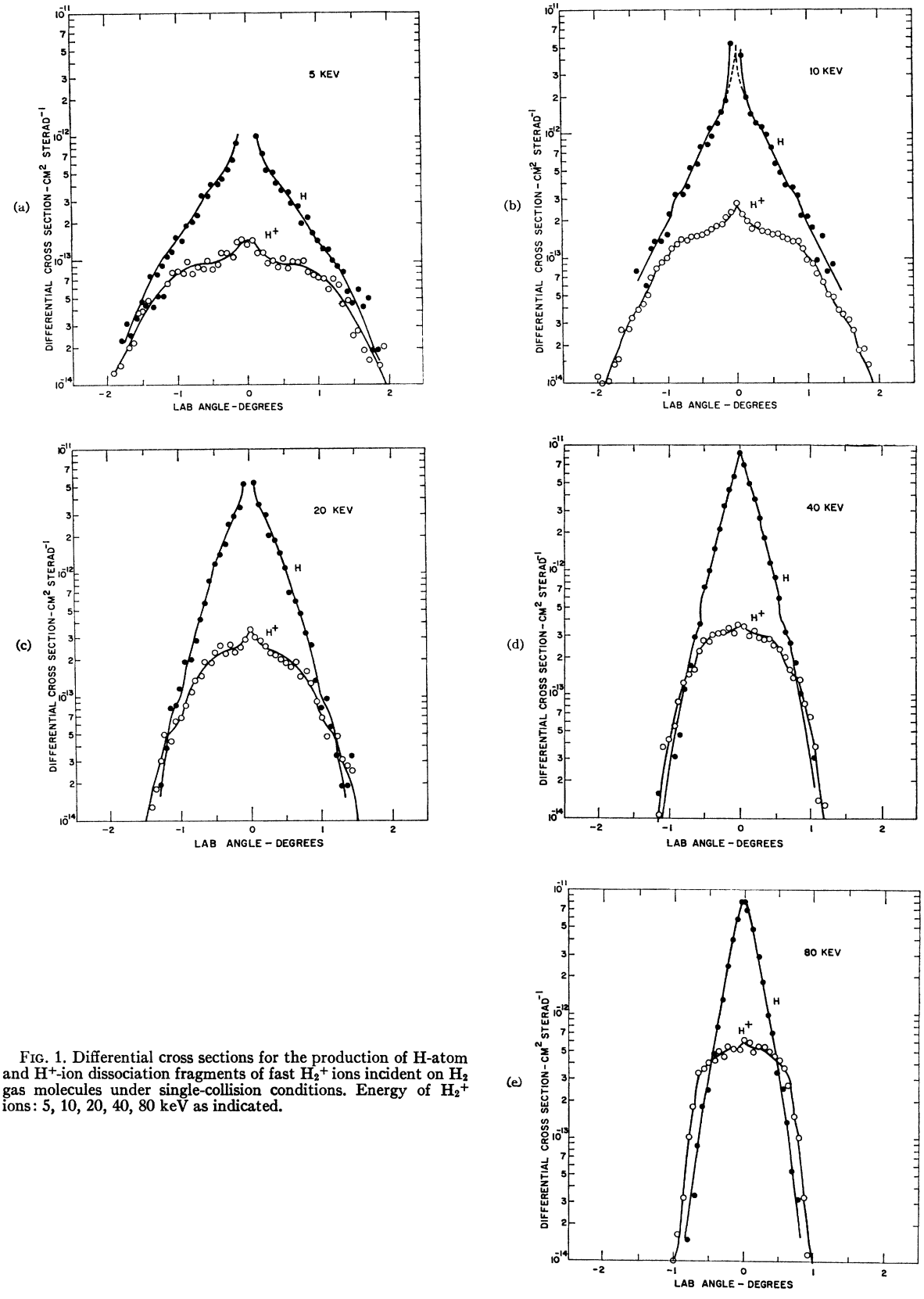

FIG. 1. Differential cross sections for the production of H-atom and H^+-ion dissociation fragments of fast H_2^+ ions incident on H_2 gas molecules under single-collision conditions. Energy of H_2^+ ions: 5, 10, 20, 40, 80 keV as indicated.

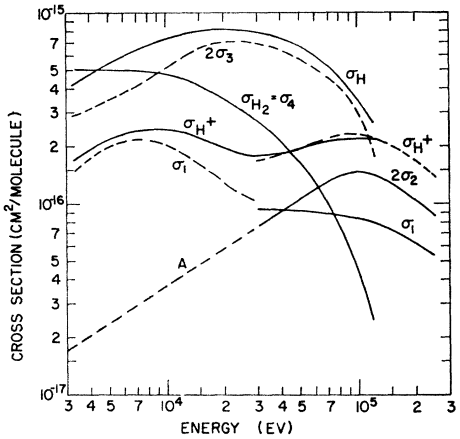

FIG. 2. Experimental cross sections for dissociation and neutralization of fast H_2^+ ions in collisions with H_2 molecules. σ_{H_2}, σ_H, and σ_{H^+} are cross sections for production of fast H_2, H, and H^+ secondaries, respectively, while σ_1, σ_2, and σ_3 are cross sections for dissociation via reactions 1, 2, and 3 noted in the text. Solid curves σ_H, σ_{H^+}, and σ_{H_2} are from McClure, Ref. 13. Solid curves σ_1 and $2\sigma_2$ are from Guidini, Ref. 8. Dashed curve σ_{H^+} is the sum of σ_1 and $2\sigma_2$. Dashed curve A is the author's extrapolation of Guidini's $2\sigma_2$ values to lower energies and dashed curve σ_1 is obtained by subtracting the extrapolated $2\sigma_2$ curve from the σ_{H^+} curve. Curve $2\sigma_3$ is derived by subtracting σ_1 from σ_H.

The central portions of the 5-, 10-, 20-keV H-atom angular distributions, where data points are omitted in Fig. 1, were found to be inaccurate because at the small angles a pronounced interference from H_2 molecules was picked up in the H-atom pulse-height channel. A correction for the H_2 interference indicated by the dotted line in Fig. 1 was made at 10 keV only. The H^+ data were unaffected by H_2 interference.

The H_2 molecules resulting from reaction 4 were practically all contained in a very narrow cone of 0.1-deg full width. As this width was of the same order of magnitude as the angular resolution, no detail could be resolved in the H_2 data.

The main result of the experimental investigation is the disclosure of clear structural features not previously observed in the H^+ and H angular distributions. Noteworthy details in the H^+ distributions are the pronounced central peaks of approximately 0.4-deg width superimposed on a broader flat-topped distribution having pronounced shoulders. The shoulders appear at $\sim\pm 1.0$ deg at 5 keV and at smaller angles as the energy is increased up to 80 keV. The H-atom distributions are very sharply peaked at zero degrees and decrease approximately exponentially with increasing angle beyond about 0.2 deg.

It is important to note that the H-atom and H^+-ion distributions have very different shapes and that the differential intensity of H atoms exceeds the differential intensity of H^+ ions by about an order of magnitude at small angles. At the largest angles observed and at low energies, the H-atom differential intensity is somewhat larger than the H^+ differential intensity, but at high energies and large angles the H^+ differential intensity exceeds the H differential intensity.

IV. DEPENDENCE OF ANGULAR DISTRIBUTION SHAPE UPON MODE OF DISSOCIATION

In order to interpret the angular distributions, it is necessary to consider the relative contribution of reactions 1 to 3 involved in H_2^+ collisional dissociation. In Fig. 2 are shown the available data on the variation of the separate cross sections σ_1, σ_2, and σ_3. Also shown are the particle-production cross sections σ_{H^+} and σ_H for the two types of secondaries H^+ and H, respectively. These are related to the reaction cross sections by the relations

$$\sigma_{H^+}=\sigma_1+2\sigma_2,$$
$$\sigma_H=\sigma_1+2\sigma_3.$$

The curves are taken from our previous data[13] and from the data of Guidini.[8] The two sets of results are mutually consistent since the curve σ_{H^+} derived by taking the sum of σ_1 and $2\sigma_2$ from Guidini's data agrees with our σ_{H^+} curve. In the absence of any available data on σ_2 below 30 keV, we have extrapolated Guidini's $2\sigma_2$ curve linearly (dashed curve A) and subtracted the extrapolated values from our low-energy σ_{H^+} data to obtain an estimate of σ_1 below 30 keV. Assuming the correctness of the extrapolation, it is apparent that σ_1 is much greater than $2\sigma_2$ in the energy range 5–10 keV and that most of the proton yield at these energies is from reaction 1. At 80 keV, the highest energy of these measurements, $2\sigma_2$ is greater than σ_1, therefore, reaction 2 dominates the proton production at this energy.

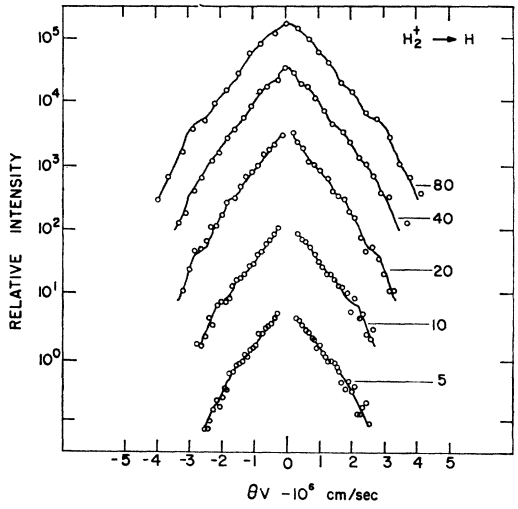

FIG. 3. Distribution of transverse velocity of H-atom dissociation fragments. Abscissa values are transverse velocities obtained from Fig. 1 by multiplying H-atom scattering angle θ by incident H_2^+-ion velocity v. Numbers attached to curves indicate primary H_2^+-ion energy in keV. Each curve was plotted after multiplication of cross-section values by an arbitrary factor chosen to avoid overlap of the plotted curves.

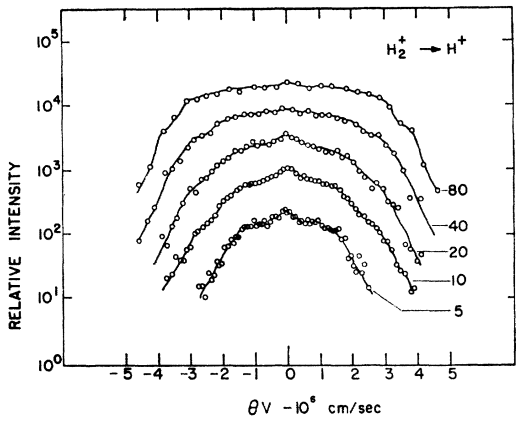

FIG. 4. Distribution of transverse velocity of H^+-ion dissociation fragments. Abscissa values are transverse velocities obtained from Fig. 1 by multiplying H^+-ion scattering angle θ by incident-ion velocity v. Numbers attached to curves indicate primary H_2^+-ion energy in keV. Each curve was plotted after multiplication of cross-section values by an arbitrary factor chosen to avoid overlap of the plotted curves.

In a similar manner, one may subtract σ_1 from σ_H to obtain $2\sigma_3$. This procedure shows that the H-atom production σ_H is dominated by reaction 3 at all energies covered by the present measurements.

As a result of these considerations, it appears that the sharply peaked H distributions are characteristic of reaction 3, while the flat-topped H^+ distributions arise from reaction 1 at low energies and from reaction 2 at high energies.

V. TRANSVERSE VELOCITY DISTRIBUTION OF DISSOCIATION FRAGMENTS

Both the H_2^+ projectile ion and the H_2 target molecule may undergo electronic and vibrational excitation in the collisions under investigation. Generally, such excitation will amount to only a few tens of eV. As this energy is small compared to the kinetic energy of the incident ions at all energies of concern here, it may be assumed that the dissociation fragments possess the same magnitude of velocity after the collision as the parent ions possessed before the collision. Thus the velocity component of the dissociation fragments transverse to the incident beam direction after the collision is given by $v\theta$ where v is the incident H_2^+ ion velocity and θ is the observed scattering angle in radians.

Transverse velocity distributions obtained by multiplying the angle scales of Fig. 1 by the appropriate values of v are shown in Figs. 3 and 4. It is seen that the H atoms possess transverse velocity distributions approximately independent of the energy of the incident ions over the 5- to 80-keV energy range, while the H^+ ions increase in transverse velocity as the beam energy increases.

Hence, in view of the results of the last section, the following relationships exist between the velocity distributions and dissociative reactions:

1. Reaction 3, which dominates the H production over the whole energy range, gives rise to a nearly invariant transverse velocity distribution over the 5- to 80-keV energy range.
2. Reaction 1, which dominates the H^+ production at low energies, gives a broader distribution of transverse velocities than reaction 3.
3. Reaction 2, which dominates the H^+ production at high energies, gives a broader distribution than either of the other two reactions.

VI. THEORY

It is the object of this section to calculate an approximate theoretical angular distribution for the H and H^+ dissociation fragments resulting from the collisional excitation of a fast H_2^+ ion from the $1s\sigma_g$ ground state to the $2p\sigma_u$ first excited state. The total potential energy versus nuclear separation for these and several other possible final electronic states of the projectile are shown in Fig. 5.

The mechanism of the dissociative event is assumed to be as follows: An incident ion enters the collision in the $1s\sigma_g$ state at a certain nuclear spacing R and undergoes an electronic transition to the $2p\sigma_u$ state. The transition is assumed to be a "vertical" one such that the internuclear spacing remains unchanged during the collision. After the collision, the $2p\sigma_u$ repulsive potential causes dissociation into the pair $H+H^+$ and each fragment

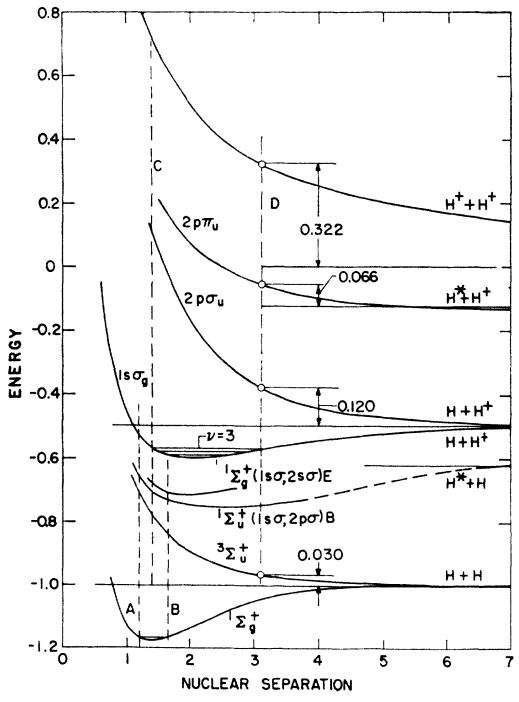

FIG. 5. Electronic energy versus internuclear spacing for several states of H_2^+ and H_2 relevant to the theoretical discussion. Energy and nuclear separation scales are in atomic units: 27.2 eV and 0.53 Å, respectively.

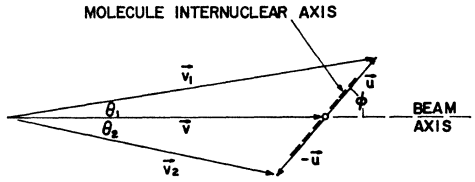

FIG. 6. Vector diagram representing a dissociative collision. Vector v is the velocity of the projectile molecule mass center before and after the collision. Vectors u and −u represent the velocities of the two dissociation fragments relative to their own mass center after the collision. Vectors v_1 and v_2 represent the velocities of the dissociation fragments in the laboratory reference frame. θ_1 and θ_2 are the laboratory angles of the dissociation fragments relative to the projectile mass-center velocity vector or beam direction. The angle of inclination of the projectile-molecule internuclear axis is denoted by φ. Since $u \ll v$, angles θ_1 and θ_2 are nearly equal. Both θ_1 and θ_2 are designated as θ in the text. The transverse velocities of the dissociation fragments are essentially $u \sin\varphi$ and the relationship $\theta v = u \sin\varphi$ is closely approximated by both fragments.

receives a kinetic energy equal to $V(R)/2$ where $V(R)$ is the potential energy of the $2p\sigma_u$ configuration at the initial spacing R minus the energy of the same configuration at $R=\infty$. This is an approximation which neglects carry-over of precollision vibrational energy to the dissociation fragments. Accordingly, the magnitude of the final velocity u of each dissociation fragment relative to the center of mass of the dissociating molecule is given by

$$u=(V(R)/M)^{1/2}, \tag{1}$$

where M is the proton mass. The final velocity vectors of the two dissociation fragments can be represented as shown in Fig. 6 by $\mathbf{v}_1=\mathbf{v}+\mathbf{u}$ and $\mathbf{v}_2=\mathbf{v}-\mathbf{u}$ where v is the velocity of the center of mass of the projectile molecule and u and −u are the equal and opposite final velocities of the two fragments relative to the center of mass of the projectile molecule. Angle φ is the angle of inclination of the H_2^+ ion internuclear axis to the beam direction, and θ_1 and θ_2 are the angles at which the dissociation fragments appear in the laboratory coordinate system. We assume that the center-of-mass velocity v is the same before and after the collision and that rotation of the molecule before and after the collision can be neglected.

The velocity component of each fragment perpendicular to the beam axis is $u \sin\varphi$. Since u is very much smaller than v in collisions of the type under consideration, the angles θ_1 and θ_2 at which the dissociation fragments appear with laboratory reference frame, are essentially identical and both angles may be accurately represented by a single quantity

$$\theta=u \sin\varphi/v. \tag{2}$$

Angle θ can be expressed as a function of v, R, and φ by substitutions of Eq. (1) in Eq. (2). Thus

$$\theta=\frac{1}{v}(V(R)/M)^{1/2} \sin\varphi. \tag{3}$$

The theoretical prediction of the laboratory-system angular distribution requires a knowledge of the cross section $\sigma(R,\varphi)$ for the $1s\sigma_g \rightarrow 2p\sigma_u$ transition as a function of R and of angle φ. Peek and Green[12] have evaluated $\sigma(R,\varphi)$ for H atom impact in the first Born approximation. In this calculation it was assumed, consistent with the results of Peek, that at 10 keV, impacts in which the H atom remains in the ground state are dominant. The results of Weihofen, Green, and Peek[14] indicate that at this energy $\sigma(R,\varphi)$ for H_2 impact should be very similar to that for H impact. In the calculation of $\sigma(R,\varphi)$ a classical, fixed-nucleus model of the heavy particles in H_2^+ was adopted. It is likely that this model, which neglects the effect of the rotation of the H_2^+ molecule as it dissociates, is adequate for the treatment of the dissociation of vibrational states of low or moderate quantum number v. However, its application to the high vibrational states is questionable.

The results of Peek's calculations for 10-keV H_2^+ ions are shown in Figs. 7 and 8. In Fig. 7 is plotted $\bar{\sigma}(R)$, the value of $\sigma(R,\varphi)$ averaged over a random distribution of molecule orientations and in Fig. 8 are plotted a family of curves representing $\sigma(R,\varphi)/\bar{\sigma}(R)$ for a selected set of R values. These plots show that the dissociation cross section is essentially independent of φ for $R \cong 3$ but is peaked at $\varphi=0$ for smaller R values and at $\varphi=\pi/2$ for large R values.

Because of the strong dependence of $\sigma(R,\varphi)$ on R, it is evidently essential to give detailed consideration to the statistical distribution of R values prior to the collision in order to predict the dissociation-fragment angular distributions. Prior to the collision, the H_2^+ ions are assumed to possess a distribution of nuclear spacings

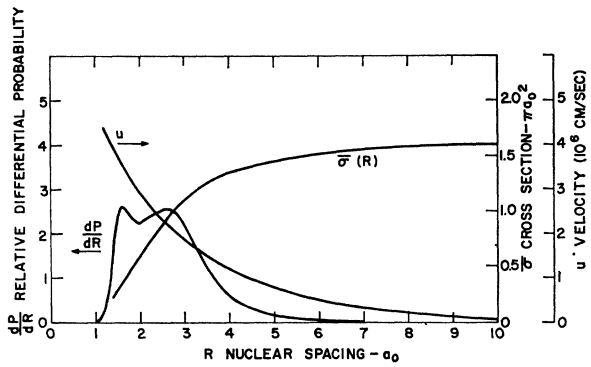

FIG. 7. Graphs of some of the functions required for the evaluation of the theoretical differential cross section. Function dP/dR is the differential probability for nuclear spacing R in the H_2^+ ion before the collision. Function u is the dissociation velocity calculated from Eq. 1 with $V(R)$ appropriate to the $1s\sigma_g \rightarrow 2p\sigma_u$ transition (Ref. 17). Function $\bar{\sigma}(R)$ is the theoretical cross section (Ref. 12) for dissociation via the $1s\sigma_g \rightarrow 2p\sigma_u$ transition with nuclear spacing R averaged over a random incident ion orientation. The dP/dR ordinate scale is arbitrary here: In the application of the theory to obtain an absolute cross section, dP/dR would be normalized so that its integral with respect to R from 0 to ∞ is unity.

[14] W. H. Weihofen, T. A. Green, and J. M. Peek (private communication).

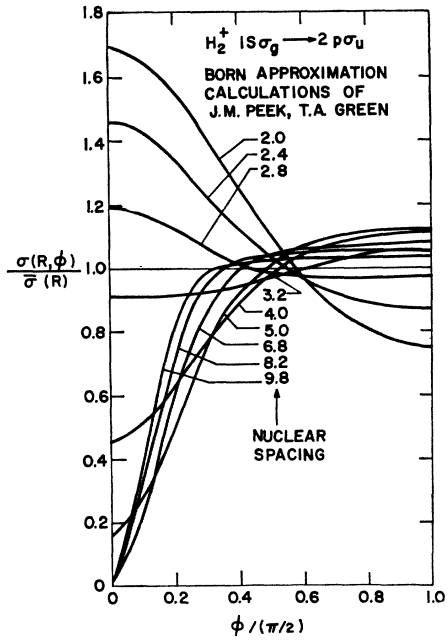

FIG. 8. Theoretical cross section for dissociation of H_2^+ ions via the transition $1s\sigma_g \rightarrow 2p\sigma_u$ for several fixed nuclear spacings R versus orientation angle φ of molecule-ion axis before collision (Ref. 12). $\bar{\sigma}(R)$ is a normalization factor defined in the text and plotted in Fig. 7. These curves apply to an H-atom target for incident H_2^+ ions of 10-keV kinetic energy.

given by

$$dP/dR=\sum_{\nu=0}^{18} f_\nu |X_\nu(R)|^2, \tag{4}$$

where $X_\nu(R)$ is the normalized vibrational wave function of the νth vibrational state and f_ν is the probability of occupancy of the νth vibrational state. The functions $X_\nu(R)$ have been calculated by Cohen and co-workers[15] and the probability factors f_ν have been calculated by McGowan and co-workers[16] for production of H_2^+ ions by electron bombardment of H_2 gas. For the present calculations the McGowan population corresponding to high-energy electrons was adopted since the choice was believed to best represent the population produced in the experimental ion source. The energy levels of the lowest four vibrational states ($\nu=0,1,2,3$) are shown in the $1s\sigma_g$ potential valley in Fig. 5 and dP/dR is plotted in Fig. 7. It is apparent from this plot that the simple assumption that all molecules have $R=2$, corresponding to the potential minimum, is not adequate for purposes of detailed analysis.

The differential cross section in the center-of-mass system for appearance of a dissociation fragment, either H or H^+, at angle φ when the H_2^+ nuclei are at spacing R prior to the collision is

$$d\sigma/d\Omega_c=(1/4\pi)\sigma(R,\varphi). \tag{5}$$

The factor $(4\pi)^{-1}$ allows for a random orientation of the H_2^+ axis with respect to the beam. From Eq. (2) the relation between the solid-angle element $d\Omega_L$ in the lab system and the corresponding solid-angle element $d\Omega_c$ in the center-of-mass system is found to be

$$d\Omega_L=(u^2/v^2)d\Omega_c\cos\varphi. \tag{6}$$

Hence, the lab differential cross section is, from Eqs. (5) and (6):

$$d\sigma/d\Omega_L=(1/2\pi)\sigma(R,\varphi)(v^2/u^2\cos\varphi), \tag{7}$$

which can be translated into a function of θ and R by substituting Eqs. (1) and (2). The factor 4 in the denominator of Eq. (5) becomes a factor of 2 in Eq. (7) because dissociations at both φ and π-φ in the center-of-mass coordinates system appear at the same angle θ, given by Eq. (3), in the lab system. The differential cross section for production of either H^+ or H alone is one-half the value given by Eq. (7).

Equation (7) gives the lab angular distribution as a function of θ for fixed R. Angle φ has the range $0\leq\varphi\leq\pi$ and hence, by Eq. (3), angle θ has the range $0\leq\theta\leq[V(R)/M]^{1/2}/v$ for small θ. Since $\cos\varphi\rightarrow 0$ and $\sigma(R,\varphi)$ is finite at $\varphi=\pi/2$, Eq. (7) is infinite at $\varphi=\pi/2$. The cross section $d\sigma/d\Omega_L$ is nevertheless integrable between the limits $\theta=0$ and the maximum value given above.

As a final step in calculating the lab-angular distribution representative of vibrating molecule ions, Eq. (7) was averaged with respect to R by performing the integral

$$\frac{d\sigma}{d\Omega_L}=\frac{1}{2\pi}\int_{R_1}^{R_2}\frac{dP}{dR}\sigma(R,\varphi)\frac{v^2}{u^2\cos\varphi}dR, \tag{8}$$

where R_1, the lower limit of the integral, was fixed at $R=1$ where $(dP/dR)\simeq 0$ and the upper limit R_2 is the solution to

$$\theta=(V(R_2)/M)^{1/2}(1/v). \tag{9}$$

All variables in the integrand of Eq. (9) can be evaluated explicitly in terms of R when θ is specified. The function $V(R)$ used in this work was taken from the results of Bates and co-workers.[17]

Results of a calculation of $d\sigma/d\Omega_L$ carried out for an H_2^+ energy of 10 keV are indicated by curve A in Fig. 9. Also shown are the experimental proton data at 10 keV. Arbitrary normalization of the theoretical calculation at 0.8 deg was employed since the total dissociation cross section calculated using $\sigma(R,\varphi)$ for an H *atom* target was about a factor of 2.7 below the estimated value of σ_1 for an H_2 target from Fig. 2. The shape of the experimental angular distribution in the neighbor-

[15] S. Cohen, J. R. Hiskes, and R. J. Riddell, Jr., Phys. Rev. **119**, 1025 (1960) and University of California Radiation Laboratory Report No. UCRL-8871, 1959 (unpublished).

[16] J. Wm. McGowan and L. Kerwin, Can. J. Phys. **42**, 972 (1964).

[17] D. R. Bates, Kathleen Ledsham, and A. L. Stewart, Phil. Trans. Roy. Soc. (London) **A246**, 215 (1953).

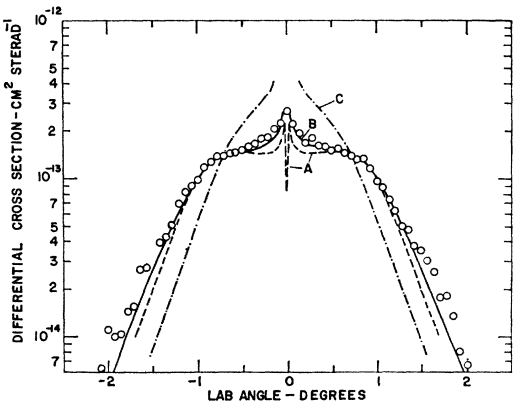

FIG. 9. Comparison of experimental proton angular distribution at 10 keV (circles) with theoretical proton angular distribution for dissociation arising from the $1s\sigma_g \rightarrow 2p\sigma_u$ transition of an H_2^+ ion striking an H-atom target. Three theoretical curves are shown corresponding to various choices of the dependence of the dissociation cross section on the H_2^+ orientation angle φ. Curve A is the theoretical result based on the functions $\sigma(R,\varphi)$ shown in Fig. 8. Curve B is the theoretical result based on an isotropic $\sigma(R,\varphi)$ such that $\sigma(R,\varphi)\equiv\bar{\sigma}(R)$. Curve C is a theoretical result based on the arbitrary assumption $\sigma(R,\varphi)\equiv\bar{\sigma}(R)\cos^2\varphi$ which would correspond to a forward-peaked center-of-mass dissociation probability.

hood of the shoulders at ~ 1.0 deg is closely followed by the theoretical curve.

The sharp minimum at $\theta=0$ in the theory is not observed experimentally and would not be clearly resolved with the angular resolution used in the present experiment. The minimum in the theory at $\theta=0$ arises from the fact that $\sigma(R,\varphi)$ (see Fig. 8) approaches zero for small φ and large R.

The local increase in the theoretical differential cross section between $\theta=0.05$ deg and 0.2 deg is similar to the local increase observed in the same angular range in the experiment. The peaking in the theoretical cross section in this angular range can be shown to be due to dissociations at $R>5.0$ and therefore to vibrational states $\nu>10$ of the H_2^+ ion. These states constitute only a very small percentage of the total vibrational population.

Also shown in Fig. 9 is the result of a calculation carried out in a manner similar to that described above except that the function $\sigma(R,\varphi)$ was arbitrarily assumed to be isotropic $[\sigma(R,\varphi)\equiv\bar{\sigma}(R)]$ instead of possessing the structure shown in Fig. 8. This evidently provides a somewhat better fit to the experimental results. No explanation is available at present.

A third theoretical curve in Fig. 9 shows the result of arbitrarily assuming $\sigma(R,\varphi)\equiv\bar{\sigma}(R)\cos^2\varphi$, corresponding to a forward-peaked dissociation preference at all R values. A considerable sensitivity of the lab angular distribution to the center-of-mass angular distribution is indicated by the three curves.

The experimental proton angular distribution falls off somewhat more slowly at angles greater than 1.2 deg than the theoretical distribution. It is possible that this is not due to any defect in the theory for the $2p\sigma_u$ dissociative mode, but rather to our failure to include consideration of the contribution of other dissociating excited states of H_2^+. In the discussion of Fig. 3, it was pointed out that reaction 2, which dominates the proton production at 80 keV, has a substantially larger transverse velocity spread than reaction 1, which dominates at 10 keV. Assuming that the velocity distributions from reaction 2 are not strongly energy-dependent, a small admixture of dissociations via reaction 2 at 10 keV would tend to make the angular distribution broader than reaction 1 processes alone. Such a contribution from reaction 2 would tend to explain the discrepancy at large angles.

If one multiplies the cross section $\bar{\sigma}(R)$ by function dP/dR, a function is obtained which measures the relative contribution of different R's to the dissociation. This product peaks at about $R=3.1$ indicating that dissociations at this spacing dominate the $2p\sigma_u$ transition. If the same thing is true of other dissociative transitions, the vertical line D drawn in Fig. 5 indicates the approximate locus along which such dissociations would occur. Typical excess energies available to the $H^+ + H^+ + e$, and $2p\sigma_u$ states are, accordingly, 0.322 and 0.120 atomic units. These correspond to dissociation velocities, calculated from Eq. (1), of 2.9×10^6 and 1.77×10^6 cm/sec, respectively. It is interesting to note that the shoulders in the 80- and 10-keV transverse velocity distributions lie very close to these respective velocities. It is not true, however, that the angular distributions can be represented accurately by a theory which invokes dissociations solely at $R=3.1$. An evaluation of the fixed-R cross-section equation [Eq. (7)] at $R=3.1$ gives an angular distribution for the $2p\sigma_u$ state which is a monatomically *increasing* function of angle out to the position of the shoulder where it reaches a sharp maximum and then drops to zero for larger angles. The contribution of R values larger and smaller than $R=3.1$ in the projectile ions is to completely fill in the central minimum in the $R=3.1$ distribution and to extend the distributions somewhat beyond the maximum θ value corresponding to $R=3.1$.

The excess energy of the pair of H atoms from the $^3\Sigma_u^+$ final state arrived at along line D would be 0.030 atomic units corresponding to a transverse velocity of 0.88×10^{-6} cm/sec. This is roughly equivalent to the mean transverse velocity represented by the relatively narrow H-atom distributions which, as pointed out above, come mainly from the electron-capture reaction 3. Absence of shoulders in the H-atom transverse velocity distributions at the calculated velocity could mean that the $^3\Sigma_u^+$ final state is strongly preferred for H_2^+ ions aligned along the beam axis, or that larger R values than $R=3.1$ dominate in the $^3\Sigma_u^+$ transition. It is also possible that $^3\Sigma_u^+$ is not the predominant final state in reaction 3; however, no state leading to the pair H+H with a smaller excess energy at $R=3.1$ is known.

It is perhaps significant that transitions to the $2p\pi_u$ state of H_2^+ at $R=3.1$ would yield a characteristic dissociation velocity of 1.31 cm/sec which is somewhat smaller than the corresponding velocity for the $2p\sigma_u$ transition. Transitions to this state might tend to raise the central portion of the experimental angular distribution and perhaps could partially reconcile the difference between the experimental data and the $2p\sigma_u$ calculation (curve A, Fig. 9) at small angles.

An effect not included in the theory presented here is the vibrational excitation process discussed briefly by Salpeter.[9] In the present type of collision, this process can manifest itself in the excitation of higher vibrational states in the H_2^+ projectile ion by close encounter between a proton of the projectile molecule and a proton of the target molecule. Two effects pertinent to the present measurements could result: (1) A certain fraction of the H_2^+ ions which are electronically excited are simultaneously vibrationally excited, and (2) a certain fraction of the H_2^+ ions are sufficiently highly excited vibrationally to enter the continuum of unbound vibrational states of the $H_2^+(1s\sigma_g)$ electronic state. Effect 1 would cause some smearing of the H^+ and H angular distributions because the dissociating fragments would possess abnormally large initial kinetic energies at the onset of the separation of the nuclei. This effect is excluded in the first Born approximation and has not been quantitatively evaluated. Effect 2 would presumably give rise to an entirely different angular distribution of dissociation fragments than that which we have calculated because, according to Salpeter's model of vibrational dissociation, dissociations with zero excess energy over the continuum boundary would be most probable while excess energies of the order of 0.120 atomic units are dominant in the $2p\sigma_u$ dissociations.

By applying Salpeter's model to the precollision vibrational population used in the present theory, we conclude that the total cross section for the process of vibrational dissociation at 10 keV is 1.7×10^{-17} cm^2. This is only 1/30 of the total collisional dissociation cross section according to the data shown in Fig. 2. While vibrational excitation does not give an important contribution to the total cross section, it may increase the differential cross section at small angles by a substantial amount. It is possible that this effect may partially explain the fact that the experimental data show a relatively large intensity at small angles as compared to theoretical curve A.

VII. DISCUSSION OF EARLIER EXPERIMENTS

Some of the past measuremeuts of the total cross sections σ_{H^+} and σ_H are in error at low energies due to the interception of a fraction of the H^+ and H dissociation fragments at the collision-chamber exit aperture. The detailed data on dissociation-fragment angular distributions presented in Fig. 1 can be used to estimate these errors where details of the apparatus geometry are known.

The measurements of McClure,[13] which encompassed all dissociation fragments within 2.2 deg of the primary beam, are not significantly in error in the energy range 10 to 120 keV. Estimated errors in the results measured at lower energies are as follows:

At 5 keV, σ_H is 9% low and σ_{H^+} is 13% low;

at 3 keV, σ_H is 17% low and σ_{H^+} is 26% low.

The estimated corrections at 5 keV are based on the assumption that the behavior of the differential cross section at angles larger than those covered in the present work is a linear extrapolation of the semilog plots shown in Fig. 1. The 3-keV corrections are based on the same type of extrapolation with the additional assumption that the 3-keV distributions (not measured) would be broader than the 5-keV distributions by a factor $(5/3)^{1/2}$. This theoretical broadening factor applies if there is a constant center-of-mass velocity distribution of dissociation fragments, independent of the energy of the incident molecule ion.

In a report by Kuprianov and co-workers[18] on the dissociation of D_2^+ ions, the collision-chamber dimensions were given along with cross-section data. According to our calculations, their collision-chamber exit aperture caused partial blockage of dissociation fragments formed at angles greater than 0.29 deg and complete blockage of fragments produced at angles greater than 0.76 deg. In an attempt to estimate the losses in this measurement, we have assumed that D_2^+ ions of energy E would behave as H_2^+ ions of energy $E/2$ in respect to the energy distribution of dissociation fragments relative to the molecule-ion mass center. According to this assumption and the present angular-distribution data, the Kuprianov measurements[18] would be in error by about 30% at 20 keV and the error would increase to about 50% at 10 keV. When corrections of this magnitude are applied to the Kuprianov data, the shape of the D^+ yield curve versus D_2^+ velocity agrees with the shape of McClure's σ_{H^+} curve versus H_2^+ velocity. This is the result one would expect assuming the same dP/dR distribution for the D_2^+ and H_2^+ ions. Although these arguments reconcile the *shapes* of the Kuprianov[18] and McClure[13] cross-section curves, there is still a discrepancy of about 30% in the magnitudes of the cross sections which may be due to calibration errors.

Large errors in gas-target-thickness determinations have been apparently involved in some of the past total-cross-section measurements. Thus, a recent report of Il'in and co-workers[19] indicates that earlier measure-

[18] S. E. Kuprianov, A. A. Perov, and N. N. Tunitskii, Zh. Eksperim. i Teor. Fiz. **43**, 1636 (1962) [English transl. Soviet Phys.—JETP **16**, 1152 (1963)].

[19] R. N. Il'in, B. I. Kikinai, V. A. Oparin, E. S. Solov'ev, and N. V. Fedorenko, Zh. Eksperim. i Teor. Fiz. **46**, 1208 (1964) [English transl.: Soviet Phys.—JETP **19**, 817 (1964)].

ments of the same group were about 50% high due to this source of error. The new σ_{H^+} values of Il'in *et al.*[19] agree well with our σ_{H^+} determinations[13] above 30 keV but fall drastically below our values at lower energies. As suggested by the authors,[19] errors in the low-energy data were perhaps caused by interception of large-angle dissociation fragments at the collision-chamber exit aperture; however, insufficient data on the collision chamber and detector geometry was given to allow us to confirm this.

Irsa and Friedman[20] concluded from mass spectrometer studies of H^+ and D^+ dissociation fragments of 4-keV HD^+ ions that the H^+ and D^+ fragments had mean transverse velocities of the order of 0.0024 times the HD^+ velocity. This result is not consistent with the present result assuming that the HD^+ ions of the earlier experiment possessed a dP/dR distribution similar to that of the H_2^+ ions used in the present experiment. Such an assumption leads to nearly an order-of-magnitude-larger angular spread than that observed by Irsa and Friedman.

[20] A. P. Irsa and L. Friedman, J. Chem. Phys. **34**, 330 (1961).

ACKNOWLEDGMENTS

The author is indebted to D. L. Allensworth for taking the experimental data, to J. M. Peek for calculating $\sigma(R,\varphi)$, and to J. M. Peek and T. A. Green for many stimulating discussions concerning the mechanism of collisional dissociation.

PHYSICAL REVIEW VOLUME 140, NUMBER 3A 1 NOVEMBER 1965

Dissociative Recombination in Neon: Spectral Line-Shape Studies*

T. Robert Connor† and Manfred A. Biondi
Department of Physics, University of Pittsburgh, Pittsburgh, Pennsylvania
(Received 1 June 1965)

Optical interferometric, spectrographic, and microwave techniques have been used to investigate the nature of electron-ion recombination in neon afterglows. Electron-density decay measurements yield a two-body recombination coefficient $\alpha \simeq 2\times10^{-7}$ cm³/sec, in agreement with earlier studies carried out at electron densities an order of magnitude smaller. The hypothesis that dissociative recombination, $Ne_2^+ + e \rightleftarrows (Ne_2^*)_{\text{unstable}} \rightleftarrows Ne^* + Ne +$ kinetic energy, is the process operative is tested by seeking to detect the kinetic energy of dissociation in the excited atoms produced by recombination. Fabry-Perot interferometer studies of the width of the λ5852 ($2p_1$-$1s_2$) neon line indicate that in the afterglow the line is very much broader than the thermal (300°K) atom width observed in the discharge. This excess width in the afterglow line is found to decrease with increasing neon gas pressure, owing to increased likelihood of excitation transfer from the fast atoms to thermal atoms before radiation. Higher-resolution studies of the spectral-line profiles indicate that the afterglow line consists of a "broad-shouldered," flat-topped component of the form expected for radiation from dissociatively produced excited atoms, surmounted by a narrow, thermal core resulting from radiation from slow-excited atoms produced by excitation transfer. The width of the fast-atom component of the profile yields a value for the dissociation kinetic energy, $E_D \simeq 1.2$ eV, leading to a binding energy for the neon molecular ion, $D(Ne_2^+) \simeq 1.4$ eV. The variation with neon pressure of slow-atom to fast-atom component in the line profile yields an excitation transfer cross section between excited $2p_1$ atoms and normal atoms of $Q_x \simeq (8\pm2)\times10^{-16}$ cm² at a relative velocity of 2.5×10^5 cm/sec. It is concluded that dissociative recombination is definitely the process responsible for the large electron loss in neon afterglows.

I. INTRODUCTION

THE present paper describes investigations designed to provide a critical test of whether or not dissociative recombination is the process responsible for the large electron loss rate observed in neon afterglows. The process of dissociative recombination was first suggested to account for the very large electron removal rates noted in ionospheric regions such as the E layer.[1] When microwave studies of noble-gas afterglows[2] gave evidence for large 2-body electron-ion recombination ($\alpha > 10^{-7}$ cm³/sec), dissociative recombination was proposed as the mechanism responsible.[3] For the case of neon, the process may be illustrated with the aid of Fig. 1 and the following equation,

$$Ne_2^+ + e \leftrightharpoons (Ne_2^*)_{\text{unstable}} \leftrightharpoons Ne^* + Ne + \text{kinetic energy}, \quad (1)$$

where the superscripts + and * indicate ionized and excited states, respectively. Thus, a molecular neon

* This research has been supported, in part, by the U. S. Office of Naval Research.

† Present address: Los Alamos Scientific Laboratories, Los Alamos, New Mexico.

[1] D. R. Bates and H. S. W. Massey, Proc. Roy. Soc. (London) **A187**, 261 (1964); **A192**, 1 (1947).

[2] M. A. Biondi and S. C. Brown, Phys. Rev. **76**, 1697 (1949).

[3] D. R. Bates, Phys. Rev. **77**, 718 (1950); **78**, 492 (1950); **82**, 103 (1951).